Kinematic model calibration of a 7-DOF capstan-driven haptic device for pose and force control accuracy improvement

Article *in* ARCHIVE Proceedings of the Institution of Mechanical Engineers Part C Journal of Mechanical Engineering Science 1989-1996 (vols 203-210) · June 2013

DOI: 10.1177/0954406212460150

2 authors:

Ozgur Baser
Süleyman Demirel University

E. Ilhan Konukseven
Middle East Technical University

JOURNAL SEARCH

Search Terms: PROCEEDINGS OF THE INSTITUTION OF MECHANICAL ENGINEERS PART C-JOURNAL OF MECHANICAL ENGINEERING SCIENCE

Total journals found: 1

THE FOLLOWING TITLE(S) MATCHED YOUR REQUEST:

Journals 1-1 (of 1)

FORMAT FOR PRINT

PROCEEDINGS OF THE INSTITUTION OF MECHANICAL ENGINEERS PART C-JOURNAL OF MECHANICAL ENGINEERING SCIENCE

Semimonthly ISSN: 0954-4062

SAGE PUBLICATIONS LTD, 1 OLIVERS YARD, 55 CITY ROAD, LONDON, ENGLAND, EC1Y 1SP

Coverage

- Science Citation Index
- Science Citation Index Expanded
- Current Contents - Engineering, Computing & Technology

Journals 1-1 (of 1)

FORMAT FOR PRINT

Proceedings of the Institution of Mechanical Engineers, Part C: Journal of Mechanical Engineering Science

P Goncalves	Pontifical Catholic University, Brazil
S T Halliday	Rolls-Royce, UK
D Hills	University of Oxford, UK
M Ishihama	Kanagawa Institute of Technology, Japan
J C Jones	University of Aberdeen, UK
A Krivtsov	St. Petersburg State Polytechnical University, Russia
L Li	University of Manchester, UK
T Lim	University of Cincinnati, USA
G Lock	University of Bath, UK
M Lucas	University of Glasgow, UK
Y Mikhlin	National Technical University 'Kharkov Polytechnic Institute', Ukraine
G Mullineux	University of Bath, UK
S A Neild	University of Bristol, UK
A Neville	University of Leeds, UK
G Niu	Tongji University, China
W M Ostachowicz	Polish Academy of Sciences, Poland
M Paul	University of Glasgow, UK
R Randall	University of New South Wales, Australia
J Reese	University of Edinburgh, UK
R Singh	Ohio State University, USA
G R Tomlinson	University of Sheffield, UK
C Truman	University of Bristol, UK
K Vafai	University of California, USA
J Warminski	Lublin University of Technology, Poland
M Wiercigroch	University of Aberdeen, UK
R Wilkinson	SSE Labs, UK

Z You	University of Oxford, UK
L C Zhang	University of New South Wales, Australia
Y Zhang	Tsinghua University, China
H Zhou	Huazhong University of Science and Technology, China

Kinematic model calibration of a 7-DOF capstan-driven haptic device for pose and force control accuracy improvement

Ozgur Baser and E Ilhan Konukseven

Proceedings of the Institution of Mechanical Engineers, Part C: Journal of Mechanical Engineering Science 2013 227: 1328 originally published online 13 September 2012
DOI: 10.1177/0954406212460150

Original Article

Institution of MECHANICAL ENGINEERS

Journal of MECHANICAL ENGINEERING SCIENCE

Kinematic model calibration of a 7-DOF capstan-driven haptic device for pose and force control accuracy improvement

Proc IMechE Part C:
J Mechanical Engineering Science
227(6) 1328–1340

DOI: 10.1177/0954406212460150
pic.sagepub.com
SAGE

Ozgur Baser and E Ilhan Konukseven

Abstract

The literature on kinematic calibration of industrial robots and haptic devices suggests that proper model calibration is indispensable for accurate pose estimation and precise force control. Despite the variety of studies in the literature, the effects of transmission errors on positioning accuracy or the enhancement of force control by kinematic calibration is not fully studied. In this article, an easy to implement kinematic calibration method is proposed for the systems having transmission errors. The presented method is assessed on a 7-DOF Phantom-like haptic device where transmission errors are inherently present due to the use of capstan drives. Simulation results on pose estimation accuracy and force control precision are backed up by experiments.

Keywords

Kinematic calibration, haptic device, force control, capstan drive, transmission error

Date received: 7 February 2012; accepted: 10 August 2012

Introduction

Certain augmented reality (AR) haptic applications require accurate positioning and precise force control, such as microsurgery and teleoperation applications with high precision requirements.[1–3] Haptic device calibration plays a vital role in these systems. There are some haptic libraries to calibrate haptic device encoder offsets. They are usually developed for specific haptic devices, such as GHOST® SDK and OpenHaptics® Toolkit for Phantom® devices, Force Dimension SDK for force dimension products and MHaptic for Haptic Workstation™.[4–7] These calibration libraries can be used to compensate inaccuracies resulting from encoder reading offsets. Offset calibration of haptic device encoder using haptic libraries alone is not sufficient for accurate positioning. There are different calibration methods found in the literature to further improve the positioning accuracy of haptic devices. Harders et al. proposed tracker-based and tracker-less haptic device calibration techniques.[8–10] Infrared optical 6-DOF tracking device is used in the tracker-based method to measure haptic stylus pose for calibration of kinematic parameters. The trackerless method uses a set of physical planar constraints to correct the haptic position and then extend this correction to the entire workspace. In this calibration method, only encoder measurements are used while the tool tip is moved on aplanar surface. In the literature, there are also different methods of trackerless calibration where single planar or two perpendicular planar calibration grids are employed.[11,12] The studies mentioned above are dedicated to Phantom haptic devices. Parallel manipulators such as Delta, Cartesian and R-Cube type mechanisms are ideal candidates to be used in haptic devices for precise positioning applications, such as 6 URS Delta-based and HIPHAD v1.0 R-Cube-based haptic devices.[13,14] However, these kinds of haptic devices also need to be calibrated. Yanhe et al.[15] proposed a self-calibration method for a Delta-based parallel haptic device. All haptic calibration studies in the literature cover only kinematic parameter calibration. None of them include the transmission errors of capstan drives and the effect of calibration on force control accuracy.

There are certain similarities between haptic and industrial robot calibration, which can be classified in two groups: model-based[16–24] and modelless.[25] Model-based calibration can be considered as a global method consisting of four sequential steps: modeling, measurement, parameter identification,

Mechanical Engineering Department, Middle East Technical University Ankara, Turkey

Corresponding author:
E Ilhan Konukseven, Mechanical Engineering Department, Middle East Technical University Ankara, Turkey.
Email: konuk@metu.edu.tr

and compensation or correction. Modeling is used to estimate end-effector poses in terms of kinematic and non-kinematic parameters, and these estimated poses are used in the identification step together with the pose measurements. The measurement systems used in the calibration are laser trackers, optical, photogrammetric, cable systems, coordinate measuring machines and the odolites.[18–20,23,25–31] Khalil et al.[31] emphasized the self-calibration method where the robot calibration can be performed without using any external measurement system. However, the performance of this method is lower than the calibration methods using external measurement systems.[31] Parameter identification is a kind of regression problem, which minimizes the error between the estimated and the measured poses. The Gauss–Newton algorithm can be used for nonlinear models.[32,33] However, Levenberg–Marquardt algorithm,[34,35] a modified version of the Gauss–Newton algorithm, is better than Gauss–Newton algorithm in case of singular or ill-conditioned matrices resulting from unidentifiable parameters, insufficient measurements and/or poor scaling issues. Compensation or correction of the errors is the final step for the robot calibration. Since the haptic handle is manipulated by the user in haptic rendering applications, updating the identified model parameters used in the controller is preferred for correction.

In haptic devices, since the force applied by the user is measured at the handle and driving torques are calculated by means of a Jacobian matrix containing kinematic parameters, the calibration improves not only positioning but also force control of a haptic device. In this study, an enhanced closed-chain calibration method including the transmission errors of capstan drives of a 7-DOF haptic device is presented and the effect of calibration on force control accuracy is analyzed experimentally. All identifiable kinematic parameters (joint offsets, link offsets, link lengths and twist angles) are identified using a linear cable encoder, which has certain advantages because of easy implementation and low cost. Additionally, the joint transmission error parameters due to the parallelogram mechanism and capstan drives are identified using external encoders attached to the output joints of the transmission mechanisms. Previously, we conducted two simulation calibration studies including capstan drive transmission errors for a Phantom Premium 1.5/6-DOF and 7-DOF haptic devices.[36,37] This article presents the experimental study for the calibration of a 7-DOF capstan-driven haptic device.

The rest of the article is organized as follows: the next section presents the importance of calibration and error sources for a 7-DOF haptic device, subsequently; the kinematic modeling and calibration procedure are presented together with simulation and experimental results. In the end, a conclusion is presented.

Error sources in the kinematic model of a 7-DOF haptic device

The 7-DOF haptic device used in this study has a hybrid type link configuration. There are two separate 3 DOF serial linkages existing at the base and at the wrist of the device, which are connected to each other with a parallelogram mechanism. In order to minimize the apparent mass of the device, a static balance is achieved for all links except for the haptic handle. The parallelogram mechanism's motor is used as a counterweight, so that extra load usage is eliminated while minimizing the apparent mass (Figure 1).

A 7-DOF haptic device is similar to a 6-DOF Phantom haptic device in terms of mechanical structure; it has only one extra DOF that corresponds to the joint of the motor (3) as shown in Figure 1. If this joint is locked at the home position, the device becomes similar to a 6-DOF Phantom haptic device. The redundant joint of the 7-DOF haptic device enables the workspace to be increased approximately 20% without compromising the other design criteria.[38] This redundancy enables the device to reach positions within the workspace with different postures. Using the redundancy and appropriate optimization techniques optimal postures can be selected for haptic device performance improvement in terms of stiffness, transparency, inertia, power consumption, singularity or obstacle avoidance.[39]

In haptic device control, the reaction force between the user and device is commonly measured at the end-effector; however, the force control is achieved by means of the torque control at each joint.[40] The torque commands and torque feedback for each joint can be calculated using the Jacobian matrix according to the desired force and measured force at the handle, respectively.[40] Therefore the deviation from the ideal kinematic parameters and joint transmission errors may cause incorrect calculation of the joint torque commands and feedbacks. This emphasizes the importance of the calibration for haptic devices.

Error sources in the kinematic model of an industrial manipulator are the deviations in link lengths, link offsets, twist angles and joint variable offsets. However, for a Phantom like haptic device, due to the capstan drive and parallelogram mechanisms, joint transmission errors should also be considered.

Capstan drives are rotary transmission elements widely used in robot mechanisms because of their low inertia, low backlash, high stiffness and simple implementation. Figure 2 shows a typical capstan drive used in haptic devices. The cable in a capstan drive is typically wrapped around the input and output drums in a figure-eight pattern to transmit the power.

The transmission error of a capstan drive mechanism results from the drum eccentricities and can be modelled.[41] The drum eccentricities, represented by

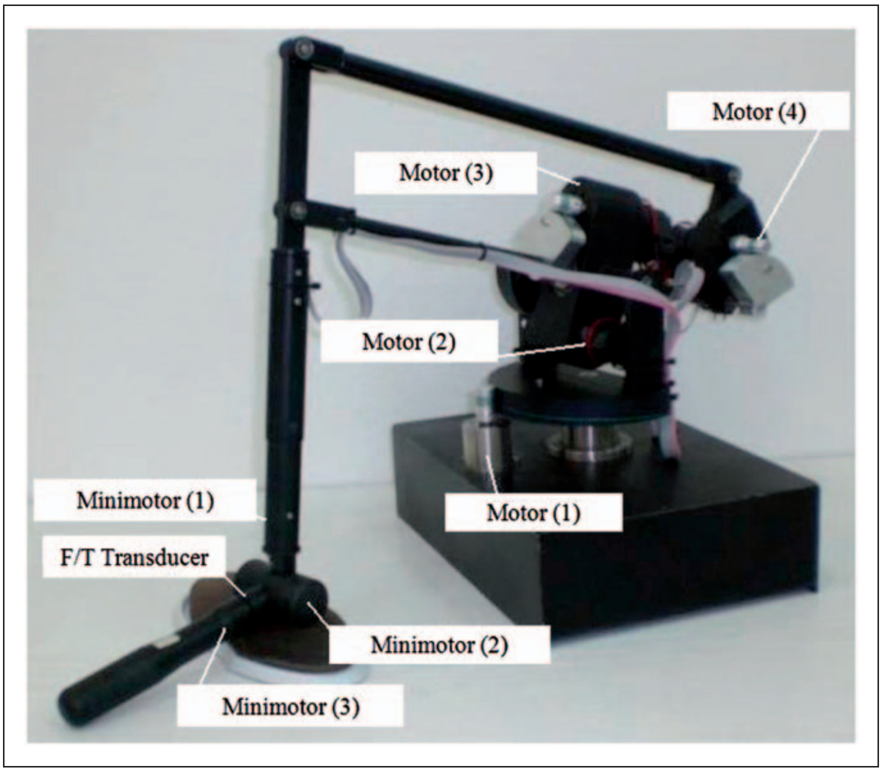

Figure 1. 7-DOF haptic device.

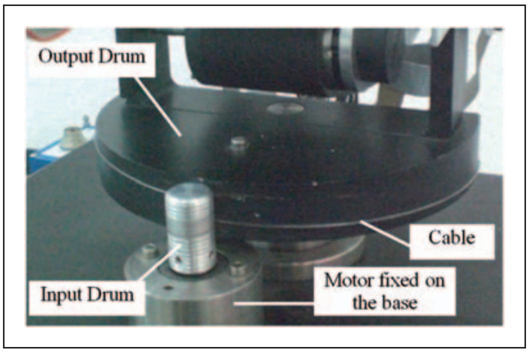

Figure 2. Capstan drive mechanism.

eccentricity radiuses (r_o, r_i) and eccentricity phase angles (β_o, β_i), are the main reasons of transmission error in capstan drives. Additionally, the error in transmission ratio and the joint variable offsets relative to the home position may cause an additional transmission error and they should be included in the calibration procedure. Equation (1) represents the mathematical model of the transmission error for capstan drives. The terms in the equation denote the transmission error due to the joint offset, transmission ratio inaccuracy, output drum and input drum eccentricity.

$$\Delta\theta_{caps} = \Delta\theta_{offset} + \Delta\theta_{ratio} + \Delta\theta_{o-ecc} + \Delta\theta_{i-ecc} \qquad (1)$$

where $\Delta\theta_{offset} = c,\ \Delta\theta_{ratio} = \left[\frac{-R_e}{R_e+R}\right]\theta$

$$\Delta\theta_{o-ecc} = \left\{ atan\left[\frac{r_o \sin(\theta+\beta_o)}{D - r_o\cos(\theta+\beta_o)}\right] - atan\left[\frac{r_o\sin(\beta_o)}{D - r_o\cos(\beta_o)}\right]\right\}$$

$$\Delta\theta_{i-ecc} = \left\{ atan\left[\frac{r_i \sin(R\theta+\beta_i)}{D - r_i\cos(R\theta+\beta_i)}\right] - atan\left[\frac{r_i\sin(\beta_i)}{D - r_i\cos(\beta_i)}\right]\right\}$$

Inaccuracy in the kinematic parameters of a parallelogram mechanism is another error source disturbing the calibration of the device. Schroer et al.[42] simplified the parallelogram mechanism by considering it as a closed-chain planar mechanism linkage. Using this technique, the calibration problem turns out to be an unconstrained optimization problem. The parallelogram mechanism used in our haptic device is considered as a planar mechanism to obtain the joint dependency.[42] The transmission error between the parallelogram joint angles (actuated and transmitted) can be formulated in terms of link lengths as follows

$$\Delta\theta_{par} = \left[\frac{L_1^2 + s^2 - L_2^2}{2L_1 s^2}\right] + \left[\frac{L_4^2 + s^2 - L_3^2}{2L_4 s^2}\right] - \frac{\pi}{2} - \theta_a \qquad (2)$$

where $s = \left(L_1^2 + L_2^2 - 2L_1L_2\cos\left(\frac{\pi}{2} - \theta_a\right)\right)$

The identification problem of the parallelograms in particular is studied by Schroer et al.[42] He reported that out of five parameters of a planar parallelogram (four link lengths and one joint angle) only one link length is identifiable.[42] The joint on the parallelogram in a Phantom-like haptic device does not require a wide range rotation (less than $\pm 45°$). Additionally, the parallelogram mechanism used in our device is actuated by a capstan drive, which complicates the transmission error model. Therefore, in our study a higher order polynomial is used to represent the transmission error of the parallelogram. Since the transmission error model of the parallelogram in 7-DOF haptic device involves ten parameters coming from the parallelogram (ΔL_1, ΔL_2, ΔL_3, ΔL_4, $\Delta\theta$) and capstan drive models (R_e, r_o, r_i, β_o, β_i), a tenth-order polynomial is selected to represent the transmission error. Note that a polynomial with a higher order than 10 might increase the computational load unnecessarily.

Kinematic modeling and proposed calibration procedure

A closed-chain calibration method is selected initially to identify kinematic parameters for easy implementation. The distance measured between the end-effector and a reference frame located on the cable encoder measurement unit is adequate for a closed-chain kinematic calibration. The accuracy of the measurement unit is limited by the maximum quantization error of the encoder. Thus it can be calculated by multiplication of the unit drum circumference and the maximum quantization error of the encoder ($\sigma_m = 2\pi R_d{*}\sigma_e = 2\pi.0.015{*}2\pi/20000$). Figure 3 shows the overall calibration setup, measurement device and its connection between the end-effector and base plate. Note that the measurement cable is connected to the end-effector by a feature presenting a link offset to identify the joint offset parameter of the last joint.

The schematic view of the 7-DOF haptic device at home position, the location of the measurement system and their coordinate frames are shown in Figure 4. The kinematic model of the structure is established using the Denavit-Hartenberg (D-H) convention.[43] A reference frame '(−1)' is attached to the starting point of the cable encoder for the closed-chain kinematic structure. The D-H parameters of the robot are given in Table 1. Note that the line connecting the robot base origin '(0)' to the measurement system origin '(−1)' is selected as the common x direction for the device and measurement system in the kinematic model. The D-H parameters of the device are given in Table 1.

In D-H convention, each homogeneous transformation matrix A_i is represented as a product of four basic transformations

$$A_i = R(z_i, \theta_i).T(a_i, 0, d_i).R(x_i, \alpha_i)R(y_i, \beta_i) \tag{3}$$

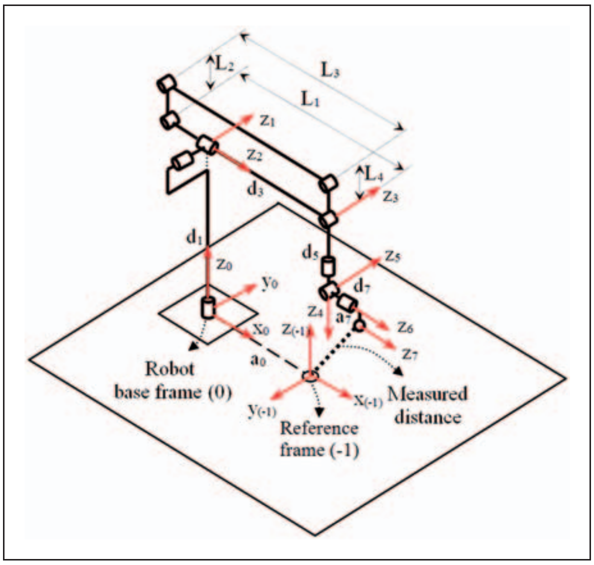

Figure 4. Kinematic model of 7-DOF haptic device for calibration.

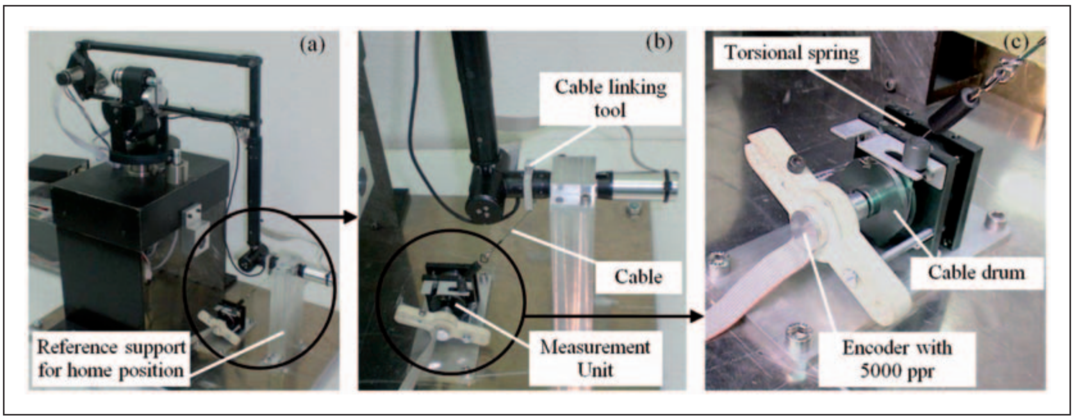

Figure 3. Implementation of the linear cable encoder in the haptic device calibration setup: (a) overall setup; (b) measurement unit connection to end-effector; (c) linear cable encoder for the distance measurement.

β_i is known as the Hayati parameter and it is used for the sequential parallel joints.[44] Since the 7-DOF haptic device does not include any parallel joints, the β_i term is not used in our kinematic model. Consequently the transformation matrix including the position ($\underline{P}$) and orientation matrix ($\underline{C}$) of the end-effector, which are relative to the reference frame attached to the starting point of the cable encoder, are given in equation (4) and the distance (δ) between the end-effector and reference frame of the measurement system is calculated from the norm of position matrix $\underline{P}$;.

$$T_0^7 = A_0 A_1 A_2 \ldots A_6 A_7 = \begin{bmatrix} \underline{C} & \underline{P} \\ \underline{0} & 1 \end{bmatrix} \tag{4}$$

$$\delta = \sqrt{P_x^2 + P_y^2 + P_z^2} \tag{5}$$

Transmission errors due to the capstan drives and parallelogram mechanism complicate the identification procedure considerably. It is not easy to identify all parameters effectively using only distance measurements in a closed-chain kinematic model. The linear cable encoder used in the experiments does not have high accuracy for the entire workspace since the measurement cable is twisted when the end-effector is pulled out from the alignment line of the measurement system ($z_{(-1)}$ axis). Therefore it is proposed that the transmission error parameters of the capstan drives and parallelogram mechanism are identified by means of external encoders attached to the output joint rotation axes. Figure 5 shows the external encoders assembled to the output joint rotation axes of the capstan drive and parallelogram mechanisms on the 7-DOF haptic device. Special parts are designed and manufactured in order to be able to assemble the external encoders on the axis of the drums (Figure 5).

Consequently the proposed calibration procedure is conducted in two sequential steps. The first one is the parameter identification and compensation of transmission errors using external encoders, and the second one is the identification and correction of kinematic model parameters using a linear cable encoder measurement system. Figure 6 shows the flowchart of this proposed calibration procedure.

Table 1. D-H parameters of 7-DOF haptic device.

Link	a_i	α_i	d_i	θ_i
w	a_0	$-\pi/2$	0	θ_0
1	0	$-\pi/2$	d_1	θ_1
2	0	$+\pi/2$	0	θ_2
3	0	$-\pi/2$	d_3	θ_3
4	0	$+\pi/2$	0	θ_4
5	0	$-\pi/2$	d_5	θ_5
6	0	$+\pi/2$	0	θ_6
7	a_7	0	d_7	θ_7

Kinematic parameter identification

In this study the actual values of the kinematic model parameters are estimated using the nonlinear least-square estimation technique. The minimization of the error between the measured distance of the closed-chain kinematic model and the computed distance using equation (5) is the base of this technique. The nonlinear least square optimization problem can be solved using the Gauss–Newton or Levenberg–Marquardt algorithm.[33] The nonlinear model of our optimization problem can be defined as given in equation (6)

$$\delta_i = f(\varphi, \eta_i) \; (i = 1, \ldots, m) \tag{6}$$

The least-square solution searches the estimate $\hat{\varphi}$ of the actual value of the parameter vector φ that minimizes the sum of squares of the error between the measured and estimated values

$$S(\varphi) = \sum_{i=1}^{m} \|\delta_i - f(\varphi, \eta_i)\|^2 \tag{7}$$

The kinematic model parameters that are not identifiable are obtained using the method presented by Khalil et al.[31] The first and last twist angles of the kinematic model (α_0 and α_7) and first joint offset (θ_0) are not identifiable since they do not have any effect on the distance measurement and calculation of the kinematic model. The line connecting the robot base origin to the cable encoder origin was selected as common the x axes in the kinematic model. Therefore, the link offset between them (d_0) is always zero and it is not included in the identification. The other (θ_0, α_0 and α_7) non-identifiable parameters are also not included in the parameter vector to be identified. However, the errors caused by them are considered in the simulation study presented in the next section.

Validity of proposed calibration method

A computer simulation was performed to show the validity of the proposed calibration procedure by using the optimization function *lsqnonlin* of the MATLAB/Optimization Toolbox®. The model parameters to be identified (referred to as the actual kinematic parameters) are generated by adding pre-defined deviations to the nominal kinematic parameters of the robot. All transmission errors are considered to be on the capstan drives and parallelogram for the definition of the virtual transmission error in the simulation. The assigned transmission error parameters and the deviations from the nominal

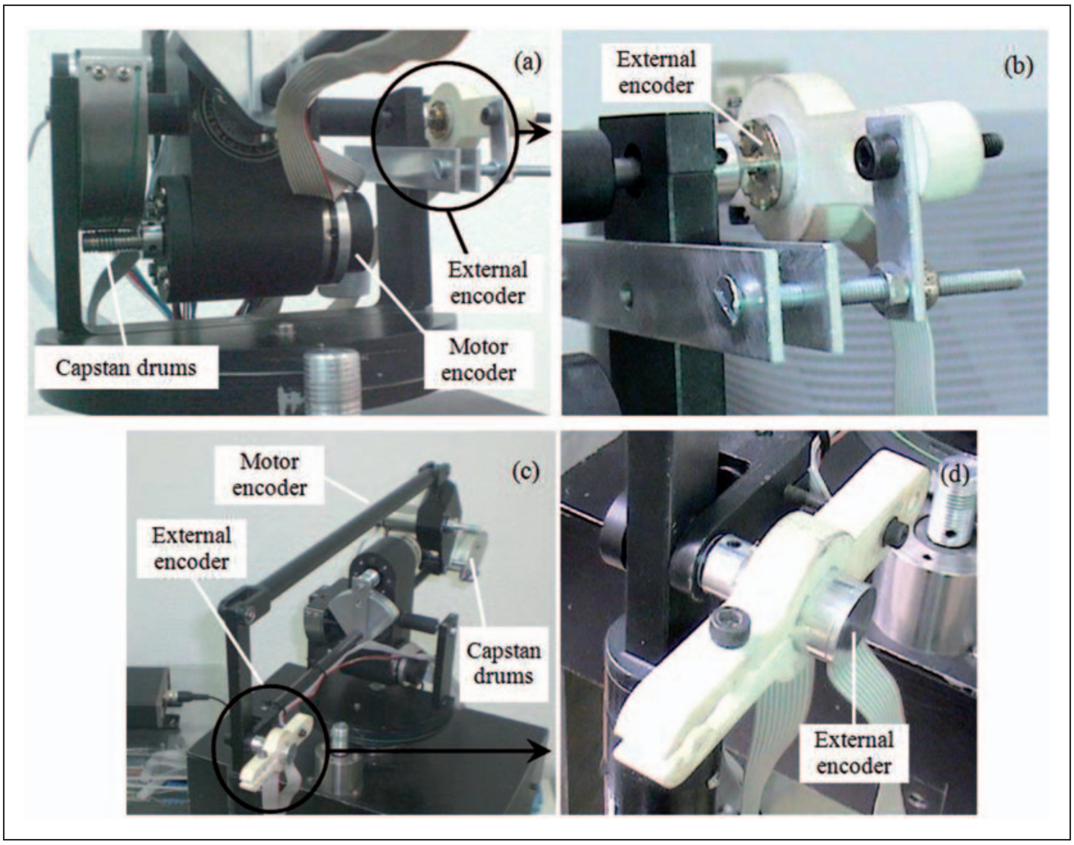

Figure 5. External encoder connections for capstan drive (a-b) and parallelogram (c-d).

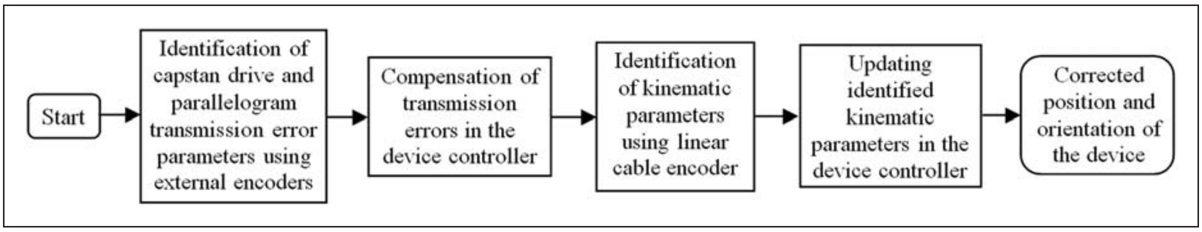

Figure 6. Flowchart of the proposed calibration procedure.

parameters are shown in Tables 2 and 3, respectively. They are assigned to characterize the parameters to be identified in the simulation. Normal noise distributions with zero mean and standard deviations are added to the output angle measurements of the transmission mechanisms and distance measurements of the closed-chain kinematic model in the calibration procedure. It is assumed that an encoder with 20,000 ppr is used in the measurement of the transmission mechanism and linear cable measurement units. The standard deviation of the encoder is taken as one-third of the maximum quantization error of the encoder ($\sigma_e = 2\pi/20000/3$). This can be used directly for the joint angle measurements of the transmission mechanisms, but for the distance measurement of the closed-chain kinematic model, it is multiplied by the cable encoder drum circumference (Figure 3(c)) ($\sigma_m = 2\pi R_d{*}\sigma_e = 2\pi.0.015{*}2\pi/20000/3$). In the simulation, 200 random pose measurements are generated with these specifications for each transmission mechanism and end-effector of the device. The identification result of the transmission mechanism model parameters and the deviations relative to the ideal kinematic model are given in Tables 2 and 3, respectively. Since transmission error of the parallelogram mechanism contains non-identifiable parameters, it is identified by using the tenth order polynomial model (Table 2).

In order to estimate how much the error of each parameter is improved, the following equation is used

$$I\ \% = \left(1 - \frac{|\lambda_a - \lambda_o|}{|\lambda_a - \lambda_n|}\right) \times 100 \tag{8}$$

$\lambda_a \neq \lambda_n$ due to the kinematic model parameter estimation errors. 100% improvement means that the

Table 2. Simulation results for the identification of the capstan drive and parallelogram parameters.

Parameters	Assigned	Identified	I (%)
Re_1	−0.025	−0.024929	99.72
Re_2	−0.020	−0.020291	98.54
Re_3	0.015	0.013933	92.89
ro_1 (mm)	0.200	0.200470	99.76
ro_2 (mm)	0.250	0.248206	99.28
ro_3 (mm)	0.200	0.209968	95.02
ri_1 (mm)	0.005	0.004968	99.36
ri_2 (mm)	0.0025	0.002522	99.12
ri_3 (mm)	0.004	0.003990	99.75
βo_1 (deg)	−105	−104.724022	99.74
βo_2 (deg)	−10	−9.921826	99.22
βo_3 (deg)	150	151.2022	99.20
βi_1 (deg)	−15	−14.585499	97.24
βi_2 (deg)	140	139.9904	99.99
βri_3 (deg)	−100	−99.1451	99.14

The parameters of fourth drum eccentricity and deviations of parallelogram	Tenth-order polynomial coefficients of the transmission error
ro_4 (mm) $= 0.1$	$k10 = 1.191804$
ri_4 (mm) $= 0.002$	$k9 = 0.633845$
βo_4 (deg) $= -40^\circ$	$k8 = -2.185038$
βi_4 (deg) $= -120^\circ$	$k7 = -0.983788$
$Re_4 = 0.02$	$k6 = 1.436945$
ΔL_1 (mm) $= -0.0005$	$k5 = 0.508398$
ΔL_2 (mm)$=-0.0007$	$k4 = -0.391253$
	$k3 = -0.100185$
	$k2 = 0.040587$
	$k1 = -0.005159$
	$k0 = 0.000043$

parameter is estimated without any error. The results are given in the last column of Tables 2 and 3. Note that α_0, α_7 are non-identifiable parameters for the proposed closed-chain model.

Since the transmission error of the parallelogram mechanism is represented by a tenth order polynomial, equation (8) cannot be used to evaluate the identification results. Therefore, the simulation measurements and identified polynomial are plotted as given in Figure 7. It shows that the identified tenth order polynomial represents the transmission error of the polynomial effectively. Note that the measurements in Figure 7 are plotted together with a noise having the same standard deviation as the encoder with 20,000 ppr.

In order to evaluate the kinematic calibration performance, 200 poses (different from those used in the identification step) are generated by using the deviated parameters before calibration and the identified parameters after calibration. Figure 8 shows the position and orientation errors together with percentage improvements in the RMS errors before and after calibration for the same poses. Note that the poses with errors over 8 mm and 0.03 rad. correspond to the joint angle sets farthest from the home position, because capstan drives produce growing transmission errors when they move away from the home position.

Based on the results, it can be concluded that the presented kinematic calibration technique is a useful and practical to improve the position and orientation of the device. Consequently, the proposed procedure can be used for the kinematic model calibration of the Phantom like haptic devices.

Experimental results

In the experimental study, while moving the device handle within the working volume the cable encoder distance measurement, the rotation angle measurements of the transmission mechanisms and the corresponding device encoder readings are recorded. During the measurement, the haptic handle is moved in such a way that almost all joints swept their entire working range within their joint limits. The identification procedure is conducted in two sequential steps as presented in the section 'Kinematic modeling and proposed calibration procedure'. 200 random measurements are selected and used in each identification procedure. The results are given in Tables 4 and 5.

Table 3. Simulation results for the identification of the kinematic parameters.

Parameters	Assigned	Identified	*I* (%)
$\Delta\alpha_0$ (mrad)	1.500	–	–
$\Delta\alpha_1$ (mrad)	−1.500	−1.477	98.47
$\Delta\alpha_2$ (mrad)	1.300	1.309	99.30
$\Delta\alpha_3$ (mrad)	−1.400	−1.396	99.73
$\Delta\alpha_4$ (mrad)	1.200	1.424	81.35
$\Delta\alpha_5$ (mrad)	−1.100	−1.320	80.01
$\Delta\alpha_6$ (mrad)	−1.600	−1.546	96.60
$\Delta\alpha_7$ (mrad)	1.700	–	–
Δa_0 (mm)	1.900	1.901	99.99
Δa_1 (mm)	−1.100	−1.089	98.97
Δa_2 (mm)	1.600	1.592	99.47
Δa_3 (mm)	−1.200	−1.199	99.99
Δa_4 (mm)	1.400	1.408	99.44
Δa_5 (mm)	−1.500	−1.499	99.99
Δa_6 (mm)	1.400	1.402	99.86
Δa_7 (mm)	−1.300	−1.301	99.99
Δd_1 (mm)	1.200	1.206	99.44
Δd_2 (mm)	−1.500	−1.504	99.71
Δd_3 (mm)	1.300	1.308	99.37
Δd_4 (mm)	−1.300	−1.269	97.64
Δd_5 (mm)	1.400	1.406	99.55
Δd_6 (mm)	−1.200	−1.201	99.99
Δd_7 (mm)	1.000	1.001	99.92
$\Delta\theta_1$ (mrad)	1.000	1.006	99.44
$\Delta\theta_2$ (mrad)	1.700	1.756	96.69
$\Delta\theta_3$ (mrad)	−1.300	−1.187	91.29
$\Delta\theta_4$ (mrad)	1.000	0.972	97.24
$\Delta\theta_5$ (mrad)	−1.200	−1.245	96.22
$\Delta\theta_6$ (mrad)	−1.000	−1.093	90.66
$\Delta\theta_7$ (mrad)	1.100	0.841	76.45

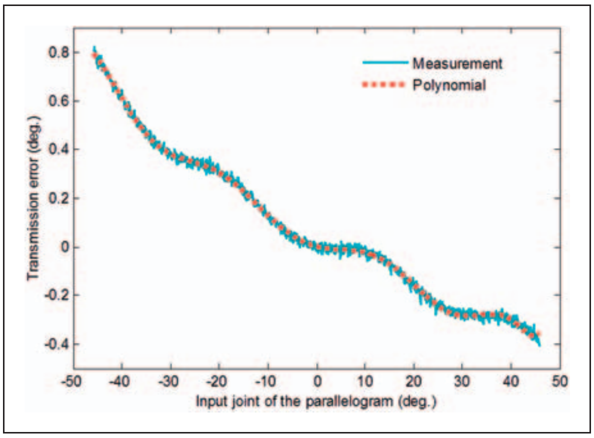

Figure 7. Parallelogram transmission error.

For each identified transmission mechanism model outputs and the corresponding measured values are plotted on the same graph as shown in Figure 9. Note that the transmission mechanism rotation angle measurement on joint axes 3 and 4 has much more noise than those of others. The noise depends on the surface roughness of capstan drive mechanisms, which jiggles the encoder readings used in the calibration.

Error compensation/correction

After the parameter identification, the next step is to improve the accuracy of the robot by making use of these identified parameters. Ideally, the identified parameters can be directly used in the device controller to correct the nominal model errors. In order to evaluate the calibration performance, the end-effector is moved randomly in the workspace for about 100 s. The calibrated and non-calibrated kinematic models are implemented on MATLAB/RealTime Windows Toolbox® using 0.001 s sampling time. The distance measured between the handle and the measurement unit and the same distance calculated using the nominal model before calibration and the corrected model after calibration are shown on the same plot (Figure 10(a)). Additionally, Figure 10(b) shows the differences between the corrected model distance errors and the non-calibrated model distance errors. The experiments were conducted for both full calibration and the calibration where the transmission errors are not included to show the effect of transmission errors on calibration. Note that the starting and finishing branches given in Figure 10 correspond to the measurements taken while the device is motionless at the home position. When the device is moved away from the home position the distance errors of the non-calibrated model rises much more relative to the calibrated model due to the transmission errors.

In order to quantify how the calibration improves the device accuracy, the percentage improvement on the root mean square of the distance errors are calculated using the formula

$$I\% = \left(\frac{|RMS(e_c) - RMS(e_{nc})|}{|RMS(e_{nc})|}\right) \times 100 \qquad (9)$$

The experiments show that the full calibration including kinematic and transmission error parameters provides 96.6% improvement in the accuracy. In order to quantify transmission error effects on the calibration results, the percentage improvement is also calculated without including transmission errors, which is found to be 44.7%. This shows that almost half of the distance errors come from the transmission errors of the capstan drives and parallelogram mechanism.

Calibration of a haptic device does not only improve pose accuracy but also the force control

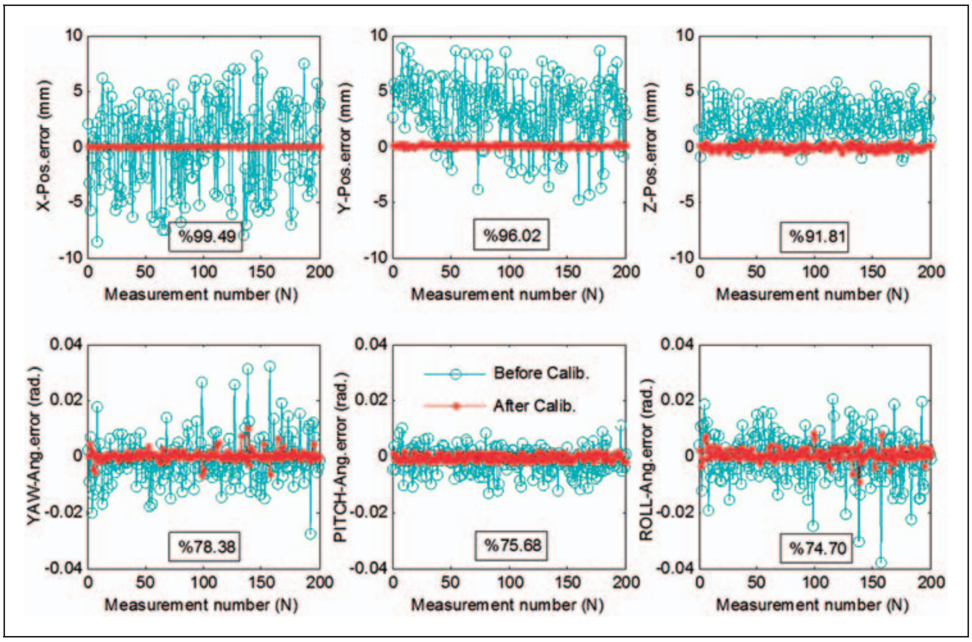

Figure 8. Calibration results for the positions and orientation angles of the end-effector of the device.

Table 4. Identification results for capstan drive and parallelogram parameters.

Parameters	Identified
Re_1	0.339383
Re_2	0.226663
Re_3	0.09557
ro_1 (mm)	1.498938
ro_2 (mm)	1.158217
ro_3 (mm)	0.3918
ri_1 (mm)	0.004212
ri_2 (mm)	0.007451
ri_3 (mm)	0.0228
βo_1 (deg)	−153.60
βo_2 (deg)	−168.40
βo_3 (deg)	−171.38
βi_1 (deg)	−110.64
βi_2 (deg)	98.00
βri_3 (deg)	80.68
Tenth−order polynomial coefficients of the transmission error	
$k10 = 4.758752$	$k4 = 0.494506$
$k9 = 3.410843$	$k3 = -0.159660$
$k8 = 5.476355$	$k2 = -0.033388$
$k7 = -3.421651$	$k1 = -0.038000$
$k6 = -2.458614$	$k0 = 0.000000$
$k5 = 1.186850$	

Table 5. Identification results for kinematic parameters.

Parameters	Identified
$\triangle\alpha_0$ (mrad)	–
$\triangle\alpha_1$ (mrad)	−2.866
$\triangle\alpha_2$ (mrad)	1.133
$\triangle\alpha_3$ (mrad)	4.550
$\triangle\alpha_4$ (mrad)	14.818
$\triangle\alpha_5$ (mrad)	−1.223
$\triangle\alpha_6$ (mrad)	−26.794
$\triangle\alpha_7$ (mrad)	–
$\triangle a_0$ (mm)	−4.195
$\triangle a_1$ (mm)	−0.402
$\triangle a_2$ (mm)	−2.966
$\triangle a_3$ (mm)	−1.225
$\triangle a_4$ (mm)	−2.584
$\triangle a_5$ (mm)	−0.076
$\triangle a_6$ (mm)	0.340
$\triangle a_7$ (mm)	−0.522
$\triangle d_1$ (mm)	−2.907
$\triangle d_2$ (mm)	2.017
$\triangle d_3$ (mm)	−3.242
$\triangle d_4$ (mm)	−0.179
$\triangle d_5$ (mm)	−1.164
$\triangle d_6$ (mm)	−1.021
$\triangle d_7$ (mm)	1.948
$\triangle\theta_1$ (mrad)	−6.088
$\triangle\theta_2$ (mrad)	5.648
$\triangle\theta_3$ (mrad)	13.363
$\triangle\theta_4$ (mrad)	−22.663
$\triangle\theta_5$ (mrad)	0.125
$\triangle\theta_6$ (mrad)	5.941
$\triangle\theta_7$ (mrad)	−51.718

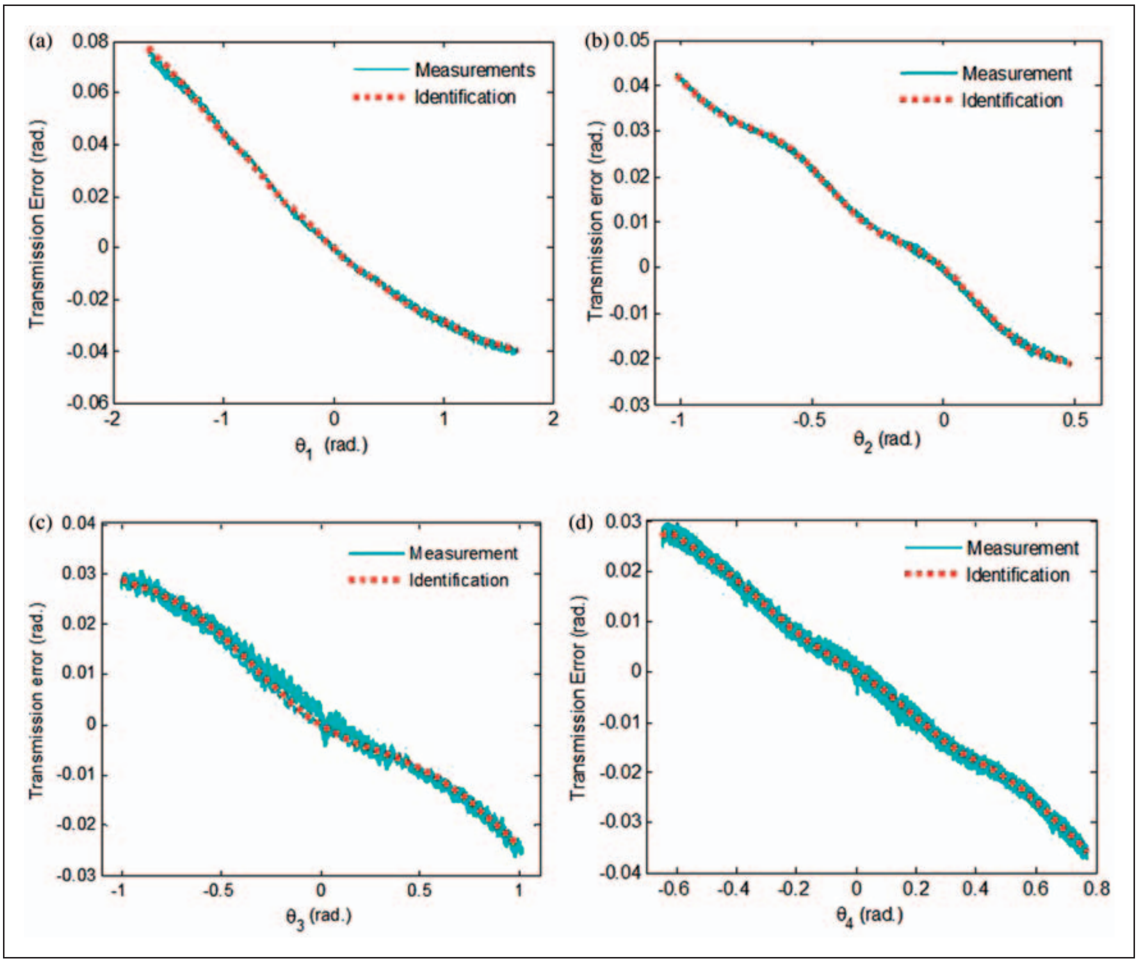

Figure 9. Identified model and measurements of transmission errors for: (a) capstan-1, (b) capstan-2, (c) capstan-3, and (d) parallelogram.

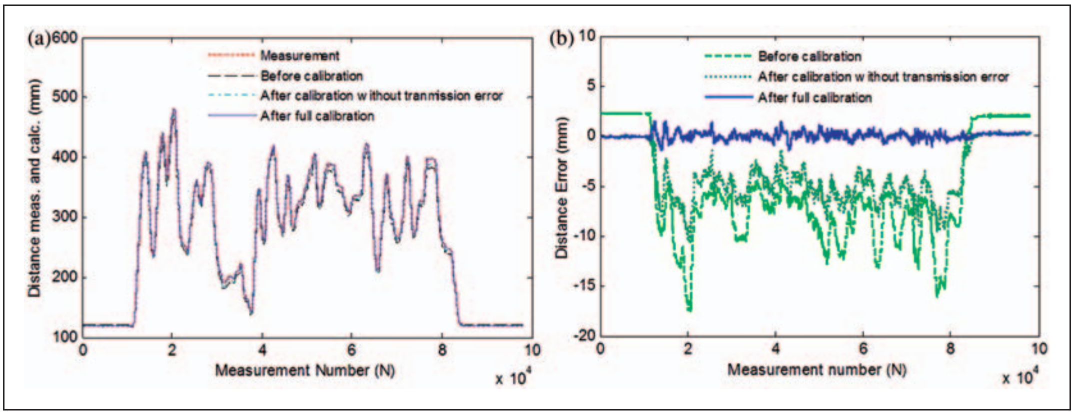

Figure 10. Distance measurement and calculations before and after calibration (a) and their errors (b).

accuracy of the device. Therefore, in this study the effect of calibration on the force control is investigated. There are two basic control algorithms in haptic interfaces; admittance and impedance control.[40] In the admittance control (AC), the motion is controlled to reflect the desired force. In the impedance control (IC), the user motion is sensed and a reference force is computed based on the virtual environment model. This type of control strategy can be improved by a force-feedback using a force transducer, which is called closed-loop impedance control (CLIC). CLIC enables to sense the virtual environment more accurately. AC and CLIC algorithms require the use of force transducers. An appropriate control algorithm can be selected based on the virtual environment and the device itself. CLIC is

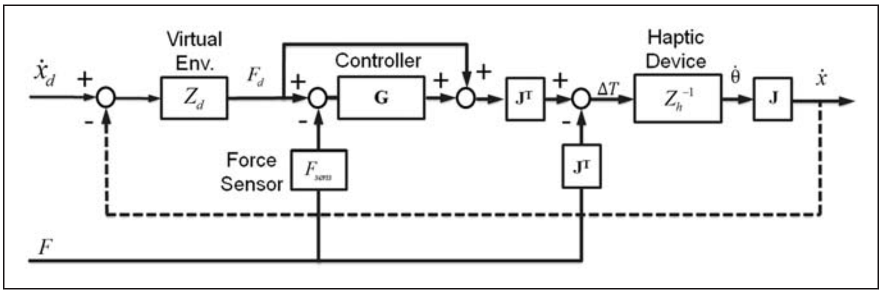

Figure 11. Closed-loop impedance control.

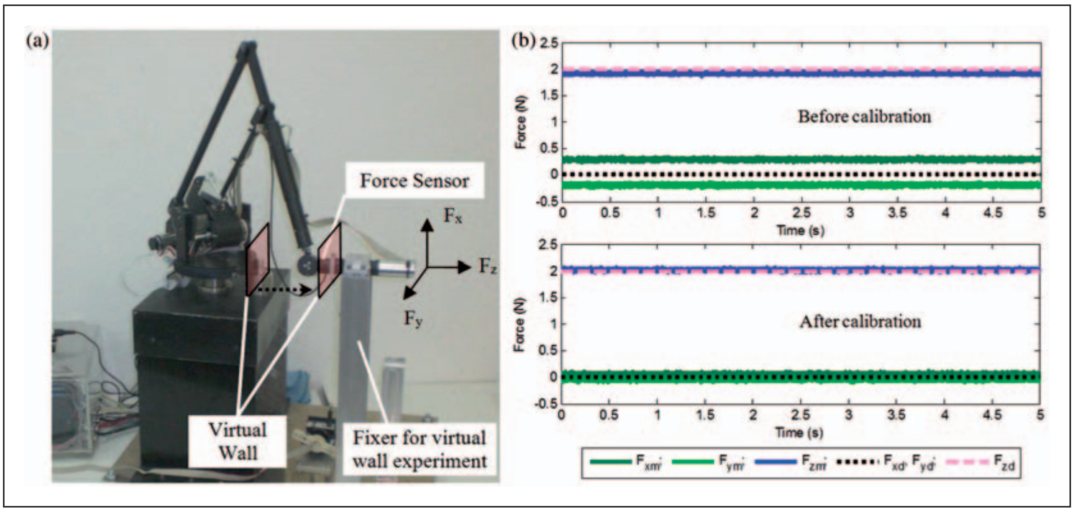

Figure 12. Virtual wall experiment of 7-DOF haptic device (a) and results of the virtual wall experiment before and after calibration (b) (m: measured, d: desired).

preferred in the haptic devices actuated by capstan drives for effective control. Figure 11 shows the block diagram of CLIC, which includes the virtual environment, haptic device, controller (Z_e, Z_h, C) and Jacobian blocks (J) as a transformer matrix between Cartesian and joint coordinates. Since the Jacobian blocks include the kinematic parameters, the calibration of the kinematic model improves the force control. The closed-loop block diagram shown in Figure 11 uses a proportional controller. McJunkin explained that it is not possible to use the other traditional (PID, PD, PI) control laws with force sensors in haptic interfaces.[45] If a force transducer is used in a PD control application, the derivative term may create difficulty due to the noise of the sensor signal. On the other hand, PI control has also practical difficulties in implementation. The PI control law can be used to correct the steady state error in a system to be controlled. However, a user who explores a haptic environment generally may not maintain static contact with an object consistently.

In order to show the effect of calibration on the force control, a virtual environment scenario is defined for an experiment. While the handle is fixed by the help of a designed fixer as shown in Figure 12(a), a virtual wall with a spring constant $K = 100$ N/m is moved 20 mm in the z-axis direction of the end-effector. In order to show the effect of calibration on the performance of controller this experiment is handled with both full calibrated and non-calibrated models. In the experiments, the reason the end-effector is fixed and the virtual wall is moved in the z-axis direction of the end-effector is to precisely provide the same position for both experiments. As a result of experiment it is expected that only a one-dimensional force is measured in the z-direction of the end-effector and the forces in the x and y directions are zero. Figure 12(b) shows the experimental results. It can be easily observed from the figure that the calibration improves the force control by eliminating the transverse forces (F_x and F_y) on the end-effector. Note that the redundant joint of the device is locked mechanically at the home position and controller parameters are the same for both experiments.

Conclusion

This study proposes an easy to implement kinematic model calibration method. Improvements on positioning accuracy and force control precision provided by the proposed method are thoroughly investigated on a 7-DOF capstan-driven haptic device containing a parallelogram. Due to the presence of capstan drives transmission errors are present in this test setup. In order to investigate the effects of kinematic calibration, a closed-chain kinematic structure is obtained by adding a linear cable encoder on to the test setup. By using this linear encoder as well as external encoders, the deviations of model parameters as well as the transmission errors are incorporated in the proposed calibration method. Effectiveness of the proposed method is investigated through simulation studies and results are validated by experiments. The obtained results indicate that, the proposed method of kinematic model calibration is not only easy to implement, but it also significantly improves the pose and force control performance of haptic devices equipped with capstan drives and parallelogram mechanisms.

Funding

The authors would like to thank TUBITAK (The Scientific and Technological Research Council of Turkey) for the funding support to manufacture the experimental setup.

References

1. Nathoo N, Çavuşoğlu MC, Vogelbaum MA, et al. In touch with robotics: neurosurgery for the feature. *Neurosurgery* 2005; 56(3): 421–433.
2. Azuma RT. A survey of augmented reality. *Presence: Teleoper Virtual Environ* 1997; 6(4): 355–385.
3. Slater M and Steed A. A virtual presence counter. *Presence: Teleoper Virtual Environ* 2000; 9(5): 413–434.
4. GHOST® SDK Programmer's Guide, Version 4.0. SensAble Technologies, Inc.,® http://www.sensable.-com/support-ghost-sdk.htm (accessed July 2012).
5. OPENHAPTICS® Programmer's Guide, Version 3.0. SensAble Technologies, Inc.,® http://www.sensable.-com/support-openhaptics.htm (accessed July 2012).
6. Force Dimension® SDK Programmer's Guide, http://www.forcedimension.com/sdk-overview (accessed July 2012).
7. Ott R, Perrot V, Thalmann D, et al. Haptic: a haptic manipulation library for generic virtual environments, In: *Cyberworlds International Conference,* Hannover, Germany, 2007, pp.338–345.
8. Harders M, Bianchi G, Knoerlein B, et al. Calibration, registration, and synchronization for high precision augmented reality haptics. *IEEE Trans Visual Comput Graphics* 2009; 15(1): 138–149.
9. Knoerlein B and Harders M. Comparison of tracker-based to tracker-less haptic device calibration, In: *IEEE World Haptics Conference,* Istanbul, Turkey, 2011, pp.119–124.
10. Bianchi G, Knörlein B, Székely G, et al. High precision augmented reality haptics, In: *Eurohaptics Conference*, Paris, France, 2006, pp.169–178.
11. Reinig K, Tracy R, Glimore H, et al. Some calibration information for a Phantom 1.5 a, In: *Proceedings of the Second PHANToM Users Group Workshop,* Cambridge, MA, USA, 1997, pp.70–73.
12. Ikits M, Hansen C and Johnson C. A comprehensive calibration and registration procedure for the visual haptic workbench, In: *Proceedings of the Joint Seventh Immersive Projection Technology and Seventh Eurographics Virtual Environments Workshop,* Zurich, Switzerland, 2003, pp.247–254.
13. Dede MIC, Selvi O, Bilgincan T, et al. Design of a haptic device for teleoperation and virtual reality systems, In: *IEEE International Conference on Systems, Man and Cybernetics*, San Antonia, Texas, USA, 2009, pp.3623–3628.
14. Sabater JM, Saltaren RJ and Aracil R. Design, modelling and implementation of a 6 URS parallel haptic device. *Robot Autonom Syst* 2004; 47(1): 1–10.
15. Yanhe Z, Jihong Y, Jie Z, et al. Autonomous kinematic self-calibration of a novel haptic device, In: *IEEE/RSJ International Conference on Intelligent Robots and Systems*, Beijing, China, 2006, pp.4654–4659.
16. Judd RP and Knasinski AB. A technique to calibrate industrial robots with experimental verification. *IEEE Trans Robot Automat* 1990; 6(1): 20–30.
17. Shiakolas PS, Conrad KL and Yin TC. On the accuracy, repeatability, and degree of influence of kinematics parameters for industrial robots. *Int J Model Simul* 2002; 22(3): 245–254.
18. Gong C, Yuan J and Ni J. Nongeometric error identification and compensation for robotic system by inverse calibration. *Int J Mach Tools Manuf* 2000; 40: 2119–2137.
19. Gatla C, Lumia R, Wood J, et al. An automated method to calibrate industrial robots using a virtual closed kinematic chain. *Proc IEEE Trans Robot Automat* 2007; 23(6): 1105–1116.
20. Mooring BW and Padavala SS. The effect of kinematic model complexity on manipulator accuracy, In: *Proceedings of the IEEE International Conference on Robotics and Automation*, Scottsdale, AZ, USA, 1989, pp.593–598.
21. Bernhardt R. Approaches for commissioning time reduction. *Ind Robot* 1997; 24(1): 62–71.
22. Caenen JL and Angue JC. Identification of Geometric and Non-geometric Parameters of Robots, In: *Proceedings of the IEEE International Conference on Robotics and Automation*, Cincinnati, OH, USA, 1990, pp.1032–1037.
23. Chen J and Chao LM. Positioning error analysis for robot manipulators with all rotary joints. *IEEE J Robot Automat* 1987; 3(6): 539–545.
24. Whitney DE, Lozinski CA and Rourke JM. Industrial robot forward calibration method and results. *ASME J Dynam Syst Meas Contr* 1986; 108(1): 1–8.
25. Wang D and Bai Y. Improving position accuracy of robot manipulators using neural networks, In: *Proceedings of the IEEE Instrumentation and Measurement Technology Conference*, Ottawa, Canada, 2005, pp.1524–1526.
26. Alici G and Shirinzadeh B. Laser interferometry based robot position error modeling for kinematic calibration, In: *Proceedings of the IEEE/RSJ International Conference on Intelligent Robots and Systems*, Las Vegas, NV, USA, 2003, pp.3588–3593.
27. Jang JH, Kim SH and Kwak YK. Calibration of geometric and non-geometric errors of an industrial robot. *Robotica* 2001; 19(3): 311–321.
28. Watanabe A, Sakakibara S, Ban K, et al. A kinematic calibration method for industrial robots using autonomous visual measurement. *Ann CIRP* 2006; 55(1): 1–6.

29. Dolinsky JU, Jenkinson ID and Colquhoun GJ. Application of genetic programming to the calibration of industrial robot. *Comput Ind* 2007; 58(3): 255–264.
30. Lightcap C, Hamner S, Schmitz T, et al. Improved positioning accuracy of the PA10-6CE robot with geometric and flexibility calibration. *IEEE Trans Robot* 2008; 24(2): 452–456.
31. Khalil W, Besnard S and Lemoine P. Comparison study of the geometric parameters calibration methods. *Int J Robot Automat* 2000; 15(2): 56–67.
32. Seber GAF and Wild CJ. *Nonlinear regression*. New York: John Wiley and Sons, 1989.
33. Hollerbach JM, Khalil W and Gautier M. Model identification. In: Siciliano B and Khatib O (eds) *Springer handbook of robotics*. Berlin: Springer-Verlag, 2008, pp.321–344.
34. Levenberg K. A method for the solution of certain non-linear problems in least-squares. *Quart Appl Math* 1944; 2: 164–168.
35. Marquardt DW. An algorithm for least-squares estimation of nonlinear parameters. *J Soc Ind Appl Math* 1963; 11(2): 431–441.
36. Baser O and Konukseven IK. Kinematic calibration of PHANTOM premium 1.5/6DOF haptic device. *Key Eng Mater* 2011; 486(1): 205–208.
37. Baser O and Konukseven IK. Kinematic calibration of a 7 DOF haptic device, In: *The 15th International Conference on Advanced Robotics*, Tallin, Estonia, 2011, pp.217–222.
38. Baser O and Konukseven EI. 7 DOF haptic device design, In: *EuroHaptics Conference*, Paris, France, 2006, pp.507–512.
39. Baser O, Konukseven EI and Balkan T. Optimal posture control for a 7 DOF haptic device based on power minimization, In: *EuroHaptics Conference*, Madrid, Spain, 2008, pp.555–560.
40. Carignan CR and Cleary KR. Closed-loop force control for haptic simulation of virtual environments. *Haptics-e* 2000; 1(2).
41. Baser O and Konukseven EI. Theoretical and experimental determination of capstan drive slip error. *Mech Mach Theory* 2010; 45: 815–827.
42. Schroer K, Albright SL and Lisounkin A. modeling closed-loop mechanisms in robots for purposes of calibration. *IEEE Trans Robot Automat* 1997; 13(2): 218–229.
43. Denavit J and Hartenberg RS. A kinematic notation for lower-pair mechanisms based on matrices. *ASME J Appl Mech* 1955; 77: 215–221.
44. Hayati SA. Robot arm geometric link calibration, In: *Proceedings of 22nd IEEE Conference on Decision and Control*, San Antonio, TX, USA, 1983, pp.1477–1483.
45. McJunkin ST. *Transparency improvement for haptic interfaces*. PhD Thesis, Rice University, US, 2007.

Appendix

Notation

a_i	link lengths
Δa_i	deviation in link lengths
$\underline{C}$	orientation matrix
d_i	link offsets
Δd_i	deviation in link offsets
D	distance between the drums
F	force applied by the user
F_{sens}	interaction force measurement
F_d	desired force in virtual environment
G	controller gain
I	percentage improvement
J	Jacobian matrix
L_i	link lengths of parallelogram
ΔL_i	deviations in parallelogram links
m	measurement number
$\underline{P}$	position matrix
r_i	input drum eccentricity radius
r_o	output drum eccentricity radius
R	capstan drive transmission ratio
R_d	cable encoder drum radius
R_e	deviation in the transmission ratio
$R(x_i, \alpha_i)$	4×4 rotation matrices around x-axis
$R(y_i, \beta_i)$	4×4 rotation matrices around y-axis
$R(z_i, \theta_i)$	4×4 rotation matrices around z-axis
$RMS(e_c)$	RMS of the errors after calibration
$\mathrm{RMS}(\mathrm{e}_{\mathrm{nc}})$	RMS of the errors before calibration
ΔT	resultant torque in joint space
$T(a_i,0,d_i)$	4×4 transformation matrix
$\dot{x}$	haptic handle velocity
$\dot{x}_d$	human hand velocity
Z_d	virtual environment impedance
Z_h	haptic device impedance
α_i	twist angles
β_i	input drum eccentricity phase angle
β_o	output drum eccentricity phase angle
δ	norm of the position matrix
δ_i	measured distance
$\Delta\alpha_i$	deviations in twist angles
θ	joint angle reading from encoder
θ_a	actuated angle of the parallelogram
θ_i	joint variables
$\Delta\theta_{caps}$	transmission error of capstan drive
$\Delta\theta_i$	joint variable offsets
$\Delta\theta_{i-ecc}$	error due to input drum eccentricity
$\Delta\theta_{o-ecc}$	error due to output drum eccentricity
$\Delta\theta_{offset}$	error due to joint offset
$\Delta\theta_{ratio}$	error due to ratio inaccuracy
η_i	input vector of joint variables
λ_a	actual value of the ith parameter
λ_n	nominal value of the ith parameter
λ_o	estimated value of the ith parameter
σ_e	maximum quantization error
σ_m	accuracy of the measurement system
φ	parameter vector to be identified